Science of Sintering, **53** (2021) 485-496

https://doi.org/10.2298/SOS2104485P

UDK: 666.3.019; 622.785; 546.714

Processing and Properties of Ceramic Yttrium Manganite Sintered by Different Methods

Milica Počuča-Nešić[1*)], Zorica Marinković Stanojević[1], Miladin Radović[2], Rogelio Benitez[2], Marko Jagodič[3], Goran Branković[1], Zorica Branković[1]

[1]Center for Green Technologies, Institute for Multidisciplinary Research, University of Belgrade, Kneza Višeslava 1a, 11030 Belgrade, Serbia

[2]Department of Materials Science and Engineering Program, Texas A&M University, College Station, TX 77840, USA

[3]Institute for Mathematics, Physics and Mechanics, Ljubljana, Jadranska 19, SI-1000 Ljubljana Slovenia

Abstract:

Intergranular and intragranular cracks that usually form during sintering of yttrium manganite ($YMnO_3$) ceramic samples hinder the densification process of this ceramic and deteriorate its magnetic and ferroelectric properties. To overcome this problem, mechanochemically synthesized $YMnO_3$ powder was sintered using two different processes: Conventional Sintering (CS) and Pulsed Electric Current Sintering (PECS). All samples were characterized by XRD, SEM and FESEM and their magnetic and ferroelectric properties were investigated. Apart from their phase composition, conventionally sintered ceramic samples showed cracks throughout their whole volume, reaching a maximum relative density of 85 %. However, it was found that PECS process could significantly reduce the presence of cracks within samples whose relative density reached 99.8 %.

Keywords*: Yttrium manganite; Pulsed Electric Current Sintering; Magnetic properties; Microstructure.*

1. Introduction

Multiferroic materials possessing two or more primary ferroic properties in the same phase are of great fundamental interest for researchers worldwide. The coexistence of ferroelectric and magnetic properties in one phase and possible control over magnetic properties with an electric field, and vice versa – electric properties with a magnetic field, also makes those materials interesting for various applications. Due to their unique properties, multiferroics, whether single phase or heterostructures, stand out as candidate materials for many devices with different functions, including information-storage devices, ferroelectric random access memories, spintronics and sensors, among others [1-6].

Rare earth manganites, $RMnO_3$ (where R represents rare earth or transition metal ion) are among the most studied multiferroic materials. Depending on the size of R ion, these materials can crystallize in two different structures – those with larger R cations usually crystallize in orthorhombic structure (space group, S.G. *Pnma*), while those with smaller R cations adopt hexagonal structure (S.G. $P6_3cm$). The size of the Y^{3+} ion lies at the "borderline", thus enabling $YMnO_3$ (YMO) to crystalize in both hexagonal (h) and

*) **Corresponding author:** milicaka@imsi.bg.ac.rs; milicaka@imsi.rs

orthorhombic (o) structure [4]. Hexagonal structure of YMO (h-YMO) consists of MnO_5 trigonal bipyramids whose bases are corner linked by oxygen ions forming triangular lattice layer in the *ab* plane. Yttrium ions are located between the layers of MnO_5 bipyramids along *c* direction [3,7-9]. On the other hand, the metastable orthorhombic YMO phase consists of a 3D framework of corner-sharing MnO_6 octahedra. The Y ions occupy the 12-coordinated interstices, formed by eight such octahedra [10].

Previous studies on multiferroic properties of both h-YMO and o-YMO, revealed that both phases were antiferromagnetic (AFM) with a ferroelectric response. According to the literature data, Néel temperature (T_N) and ferroelectric Curie temperature (T_C) for h-YMO are 80 K and 914 K respectively, while these values for o-YMO are 42 K (T_N) and 31 K (T_C) [9,11].

Various synthesis methods have been used for the preparation of YMO: solid state synthesis [3,12-15], chemical methods [2,16-18], hydrothermal synthesis [19,20] and mechanochemical synthesis [21,22]. However, the sintering of YMO appears to be a time and energy-consuming process. To prevent the formation of impurity phases, like Mn_3O_4, YMn_2O_5 and Y_2O_3, sintering process is usually divided into several long high-temperature thermal treatments with intermediate grinding steps [13,15,23-25]. Following this pattern, the sintering process can last for several days. Nevertheless, the sintering of YMO still remains challenging because of: (i) the low final relative densities and (ii) the occurrence of intergranular and intragranular cracks in sintered samples. Moure et al. reported on the preparation of YMO ceramic material with relative density of 98 % by multistep sintering in the temperature range (1350–1525) ^oC, which is the highest reported relative density of YMO to date [25]. However, even these samples contained large intragranular cracks. Major factors that influence the cracking of $YMnO_3$ are proposed to be phase transformation of o-YMO into h-YMO around 950 ^oC [26], highly anisotropic thermal expansion coefficients [27] and high-temperature phase transition from paraelectric (S.G. $P6_3/mmc$) to ferroelectric h-YMO phase (S.G. $P6_3cm$) [28]. All these processes induce large stress and as a result cracking occurs within YMO samples during sintering. Internal stress is proportional to the crystallite size, and in the case of larger crystallites, it is unevenly distributed throughout the material, contrary to the evenly distributed stress in the material with smaller crystallites. To prepare crack-free dense YMO material, researchers have proposed doping of h-YMO with Ti or Sr [3, 16]. Another possible solution of this problem could be reducing the stress distribution by decreasing the materials crystallite size.

Pulsed Electric Current Sintering (PECS)[1] has been previously used for sintering and increasing the density of various materials [29-31]. In this paper, we propose this method as a possible way of sintering crack free YMO with high density. In this method, high temperatures applied simultaneously with high pressures significantly lower sintering temperatures, leading to faster and better densification of the material and small grain sizes. Also, high heating rates with short sintering times in this process practically suppress the grain growth, resulting in the narrower distribution of smaller grains in sintered samples, when compared to conventionally sintered samples.

The aim of this study is to reach high density of the sintered YMO samples as well as to reduce the cracking of the sintered samples and possibly improve their ferroelectric properties. For this purpose, we will utilize both PECS and conventional sintering processes, and compare the properties of the obtained ceramic material.

2. Experimental

For the preparation of yttrium manganite precursor powder, denoted as YMO-PP, we used mechanochemical synthesis process. The precursor mixture, containing Mn_2O_3 (Aldrich,

[1] Commonly referred to as Spark Plasma Sintering (SPS) in the past.

p.a. 99 %) and Y_2O_3 (Alfa Aeser, p.a. 99.9 %) weighted in equimolar Y:Mn ratio, was dry milled in the air in a planetary ball mill (Fritsch Pulverisette 5) using tungsten carbide (WC) cylindrical vials (V = 250 cm^3, Dv = 75 mm) and WC balls (35 balls with d = 10 mm, ρ = 14.95 g/cm^3); ball-to-powder weight ratio was 30:1; the milling time was 6 h at the rotational speed of disc of 120 rpm.

Sintering of YMO-PP was performed by two methods: Conventional sintering (CS) and Pulsed Electric Current Sintering (PECS).

For the CS process, as-prepared powder was uniaxially pressed into pellets (Ø = 8 mm) at 785 MPa. In order to optimize the sintering conditions, conventional sintering was performed in a chamber furnace in ambient air using three different regimes: (1) at 900 ^oC for 2 h (sample denoted as YMO-CS-A); (2) at 900 ^oC for 2 h followed by treatment at 1100 ^oC for 12 h with intermediate grinding between two sintering steps (sample denoted as YMO-CS-B) and (3) at 1400 ^oC for 2 h (sample denoted as YMO-CS-C). In all those processing regimes samples were heated at the rate of 10 ^oC/min.

PECS process was performed in the Model # SPS 25-10 (Thermal Technology LLC) using a graphite die with the diameter of 16 mm, under the constant flow of the ultra-high purity argon. Sintering temperature was 1100 ^oC with the heating rate of 100 ^oC/min, while the sintering time was 10 minutes. Uniaxial pressure of 60 MPa was applied before the heating cycle and maintained until the sample cooled down to room temperature at cooling rate of 100 ^oC/min. For the compensation of possible oxygen-nonstoichiometry after PECSing in the inert atmosphere, the sample was annealed at 1200 ^oC for 4 h in ambient air, using heating rate of 10 ^oC/min, and cooling rate of 5 ^oC/min. This sample was denoted as YMO-PECS.

X-ray powder diffraction (XRD) analysis of prepared precursor powder and sintered samples was determined using Rigaku Ultima IV, Japan, with CuKα radiation (λ = 0.154 nm) from 15 ° to 70 ° (2θ). *PowderCell* (version 2.4) software was used for the phase composition analysis [32]. The microstructural characterization was performed by field emission scanning electron microscopy (FESEM, Jeol JSM 6330F) and scanning electron microscopy (SEM, TESCAN Vega, TS 5130 MM).

The magnetic measurements of the YMO ceramic samples were carried out with a SQUID MPMS-XL-5 magnetometer from Quantum Design. The zero-field-cooled (ZFC) and field-cooled (FC) magnetization vs. temperature curves were collected in the temperature range 2-300 K, while isothermal magnetization measurements were recorded between -50 and 50 kOe at two temperatures, 5 and 2 K.

Standard bipolar hysteresis measurements of the ceramic samples coated with gold paste were performed on Precision Multiferroic Test System (Radiant Technologies, Inc.), consisting of Multiferroic Test Unit and the High Voltage Amplifier. The hysteresis period was 10 ms and the applied fields were in the range of (5-50) kV/cm.

Inductively coupled plasma optical emission spectrometry (ICP-OES) measurement was performed using Thermo Scientific iCAP 6500 Duo ICP (Thermo Fisher Scientific, Cambridge, United Kingdom).

3. Results and Discussion

3.1 XRD Analysis

The XRD pattern of YMO-PP in Fig. 1a confirms presence of only orthorhombic $YMnO_3$ phase (PDF # 20-0732, space group *Pbnm*) in synthesized powders and no peaks belonging to any other phase can be detected (Table I). Therefore, long milling time used in this study introduced enough energy in the reaction system to complete the mechanochemical reaction and form pure o-YMO [22].

The preparation of ceramic bulk, dense samples of metastable o-YMO usually starts from the hexagonal YMO as a precursor and requires high pressures and high sintering temperatures [1,33-35]. Still, some published results suggest that this phase could also be prepared at lower temperatures [16]. It is also known that o-YMO is the first phase to crystallize during the sintering process of YMO [16]. Following these ideas, our first attempt in the preparation of dense, crack free yttrium manganite was to maintain the phase purity of YMO-PP and prepare o-YMO bulk samples. For this reason we selected 900 ^{o}C as a starting sintering temperature for conventional sintering, which is lower than the phase transformation temperature from o-YMO to h-YMO [17,36,37]. However, this process resulted in samples containing o-YMO (JCPDS # 20-0732, S.G. *Pbnm*) as a major phase, and h-YMO (JCPDS # 25-1079, S.G. *$P6_3cm$*) as a secondary phase (Fig. 1a, Table I). This finding is in good agreement with that reported by Liu et al., who also found presence of both YMO phases after sintering at similar conditions [38]. In our case, samples sintered by CS-A process also had very low relative densities, less than 60 % and they were not further analyzed. Therefore, we can conclude that it is impossible to prepare pure ceramic o-YMO samples by sintering at temperatures as low as 900 ^{o}C.

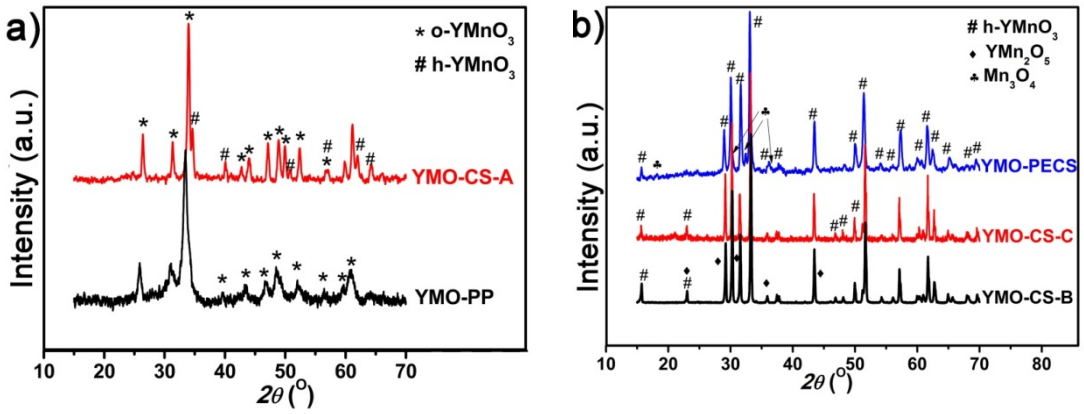

Fig. 1. XRD patterns of YMO-PP and ceramic samples sintered by CS and PECS methods: (a) YMO-PP and YMO-CS-A and (b) YMO-CS-B, YMO-CS-C and YMO-PECS.

Tab. I The phase composition of YMO ceramic samples sintered by conventional and pulsed electric current sintering methods based on the Powder Cell refinement.

Sample →	YMO-PP	YMO-CS-A 900^{o}C/2h	YMO-CS-B 900^{o}C/2h 1100^{o}C/12h	YMO-CS-C 1400^{o}C/ 2h	YMO-PECS 1100^{o}C/10min
o-YMO [wt.%]	100	89.9	0.0	0.0	0.0
h-YMO [wt.%]	-	10.1	97.4	100	97.8
YMn_2O_5 [wt.%]	-	-	2.6	-	-
Mn_3O_4 [wt.%]	-	-	-	-	2.2
Relat.density [%]	-	62	74	85	99.8

In our second attempt to prepare single phase ceramic material with higher densities, we also sintered YMO-PP powder using two-step sintering process. The first sintering step was indeed the same as in CS-A process, followed by crashing and pulverization of the obtained pellets. The obtained powder was then uniaxially pressed and sintered at 1100 ^{o}C for a longer period of time (24 h). These sintering conditions enhanced the relative densities of the obtained samples, but only to 74 % (Table I).

According to the XRD pattern, YMO-CS-B ceramic samples consist of well-crystallized h-YMO (JCPDS # 25-1079, S.G. *P6$_3$cm*) and orthorhombic YMn_2O_5 (JCPDS # 34-0667, S.G. *Pbam*) as the secondary phase (Fig 1b, Table I). We could hardly avoid the formation of orthorhombic YMn_2O_5 since this phase is stable up to 1100 ^oC [7,39], but above this temperature, it decomposes into h-YMnO and ferrimagnetic Mn_3O_4 [7,21], which can deteriorate the samples magnetic properties. On the other hand, YMn_2O_5 is also an antiferromagnetic material, so we did not expect it to influence significantly the materials magnetic properties.

Simultaneous rising of the sintering temperature to 1400 ^oC and reducing the sintering time in order to suppress the abnormal grain growth was our third attempt to prepare dense single-phase YMO ceramics. The analysis of XRD for this ceramic sample revealed presence of single phase h-YMO (Fig. 1b, Table I), since all peaks can be attributed solely to h-YMO (JCPDS # 25-1079, S.G. *P6$_3$cm*). The relative density of these ceramic samples was 85 %, and it was the highest density of all conventionally sintered samples in this study.

To further enhance the density of ceramic samples, as our fourth attempt, we applied the PECS process for the sintering of YMO-PP. As a very efficient method for the sintering and densification of ceramic materials, PECS wasn't much used in the synthesis of yttrium manganite, except for the studies published by Ma *et al.* [40] and Wang *et al.* [41]. XRD analysis of our pulsed electric current sintered samples (Fig. 1b) revealed that obtained samples contain h-YMO (JCPDS # 25-1079, S.G. *P6$_3$cm*) as the main phase, with small quantity of Mn_3O_4 as a secondary phase (Table I). Since the whole process is conducted in the reduction atmosphere, the sintering conditions enabled the formation of Mn_3O_4. In this case, the reduction of manganese occurs with the change of its oxidation state from Mn^{3+} to Mn^{2+}, with simultaneous oxidation of carbon from the graphite mold in which the powder is placed during the sintering process. As we expected, ceramic samples obtained by the PECS process have the highest relative density, reaching the value of 99.8 %, which is higher than in the case of other PECS sintered YMO reported before [40,41].

3.2 Microstructural analysis

Microstructural analysis of YMO-PP reveals the presence of submicronic particles (Fig. 2a). However, it is clear from SEM images in Fig. 2a that mechanochemical treatment induced agglomeration in the precursor powder. Our previous investigations revealed that mechanochemically treated YMO powder milled for 360 min have bimodal particle size distribution with median particle size being ~2 μm [22].

SEM images of the ceramic samples prepared by the CS-B process reveal the presence of irregularly shaped grains and broad grain size distribution (Fig. 2b). As expected, sintering of the agglomerated powders resulted in samples with larger grains, up to 5 μm in their size. Microstructure of the YMO-CS-C sample (Fig. 2c) shows similar microstructural features as the YMO-CS-B sample sintered at lower temperature, i.e. larger and irregularly shaped grains, but with the larger grain size ranging from 2 to 10 μm. These micrographs also confirm the enhancement of the densities with the rise of the sintering temperature and prolongation of the sintering time. Intergranular porosity of the sample sintered at 1400 ^oC is much lower than in the case of the sample sintered at a lower temperature. Still, none of these conventional sintering conditions reduced the formation of intergranular and/or intragranular cracks that can be clearly observed in Fig. 2b and 2c.

Fig. 2d shows the free surface of the annealed ceramic sample sintered by PECS. The microstructure of this sample is far better than that of conventionally sintered samples, showing better uniformity and smaller grain size, and very few intergranular pores (in triple points) and microcracks. As a consequence of combination of high heating rate, high pressure and low sintering time, this sample shows the narrowest grain size distribution, with the grain size of ~ 2.4 μm, regardless of the fact that the starting powder used for PECSing also

contained agglomerates. In fact, this gran size is very close to the particle size of the starting YMO-PP powder, suggesting that grain growth did not take place during PECS sintering.

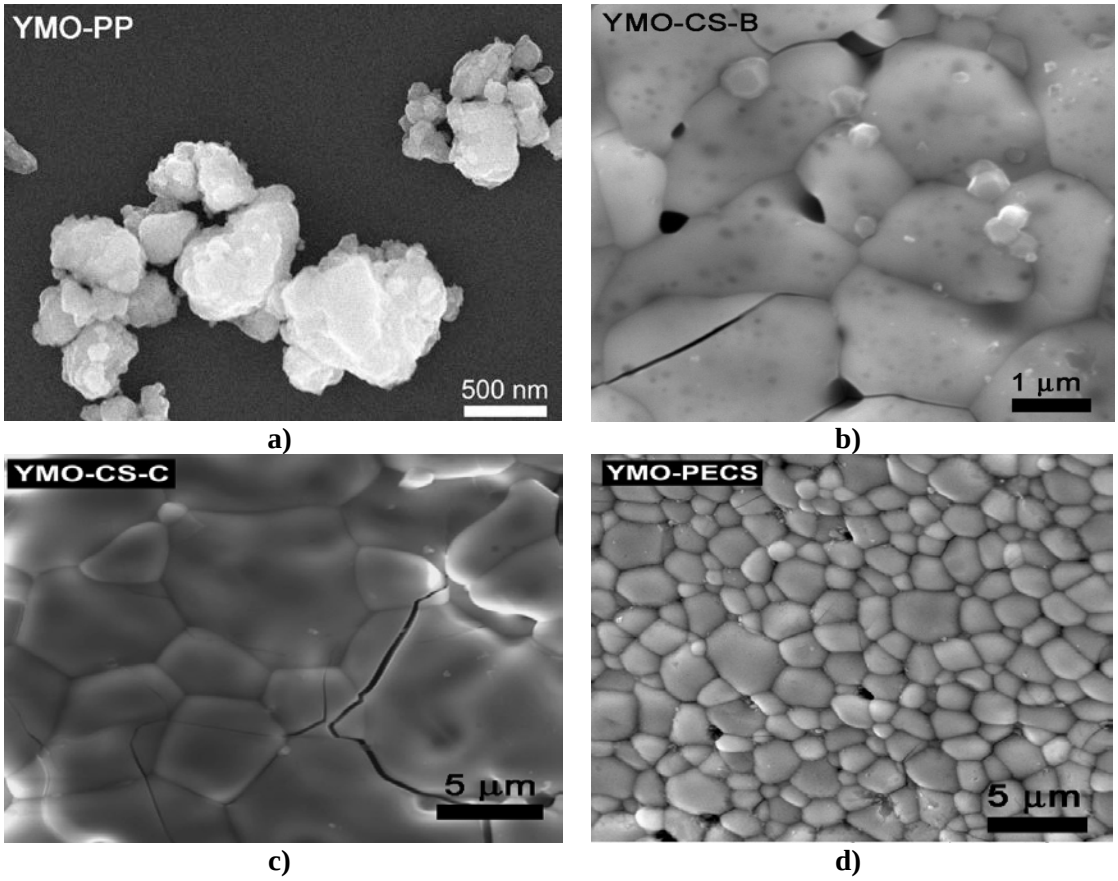

Fig. 2. FESEM micrograph of the YMO-PP (a) and scanning electron micrographs of the surface of ceramic samples: YMO-CS-B (b), YMO-CS-C (c) and YMO-PECS (d).

Although some previous studies reported cracking of the thermally etched YMO surfaces and absence of any cracks on chemically etched surfaces [25], in this study cracks appeared on free sample surfaces of all ceramic samples which were not etched in any way. It is obvious that dense and crack-free YMO ceramic material cannot be obtained by the conventional sintering process, since phase transformations during thermal treatment and highly anisotropic thermal expansion coefficients contribute to large internal stress and consequently to cracking of the material. On the other hand, pulsed electric current sintering with its heating mechanism under a uniaxial pressure enhanced densification and significantly reduced the crack formation and propagation.

3.3 Magnetic properties

Characterization of magnetic properties was performed for all samples with relative densities above 70 %, and the results for conventional sintered samples are presented in Fig. 3. Since YMO is an antiferromagnetic material, it is expected that magnetization would show a linear dependence on the applied magnetic field at temperatures lower than materials T_N.

However, isothermal curves of magnetization, $M(H)$ recorded at 2 K and 5 K for YMO-CS-B and YMO-CS-C samples respectively (Fig. 3a) are mildly S-shaped, having very low values of the coercive field (Table II). Also, low remanent magnetization and lack of

saturation indicate that ceramic material has basically antiferromagnetic characteristics with a very low weak ferromagnetic response.

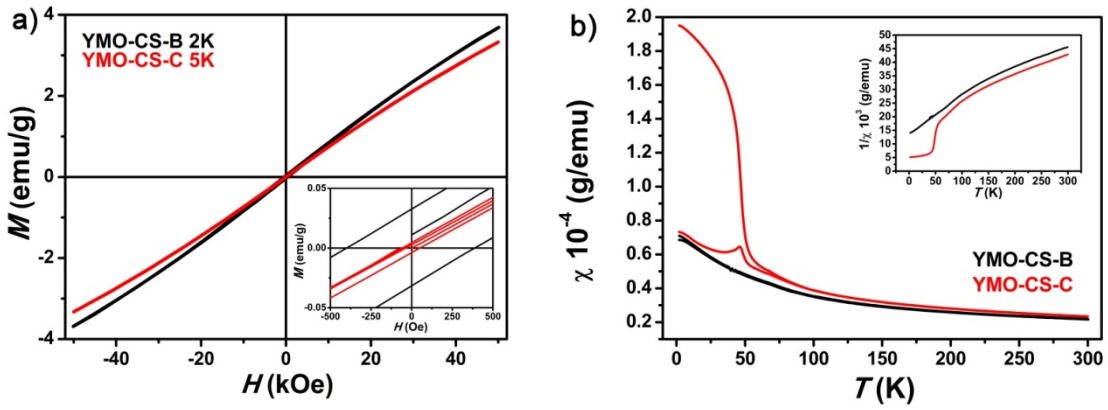

Fig. 3. Magnetic properties of the ceramic samples prepared by CS-B and CS-C sintering process: a) $M(H)$ curves (insets show low field magnetization behavior); b) Susceptibility as a function of temperature, ZFC and FC cycles, measured under an applied field of 100 Oe. (Inset shows the thermal evolution of the inverse susceptibility for YMO-CS-B and YMO-CS-C samples).

Tab. II Different parameters deduced from the magnetization curves of conventionally and pulsed electric current sintered ceramic YMO samples.

Sample	T_N [K]	Hc [Oe]	θ_{CW} [K]	μ_{eff} [μ_B]	M_R [emu/g]
YMO-CS-B	72	49	-353	4,67	0.004
YMO-CS-C	45	390	-272	4,50	0.03
YMO-PECS	43	2500	-130	4.4	0.64

T_N, Néel temperature (antiferro-paramagnetic transition); *Hc*, coercive field measured at 2K or 5 K; θ_{CW}, the paramagnetic Curie–Weiss temperature; μ_{eff}, effective magnetic moment; M_R remanent polarization.

ZFC and FC curves of the ceramic sample obtained by the CS-B process, overlap through almost entire temperature range without any significant bifurcation or separation. The high temperature overlapping indicates paramagnetic behavior at these temperatures. Néel temperature of this sample, obtained from the inverse susceptibility vs. temperature curve is close to the literature data for the dominant phase present in these samples, *i.e.* h-YMO. By fitting the inverse susceptibility vs. temperature curves (Inset Fig. 3b) with the Curie –Weiss law, $\chi=C/(T-\theta_{CW})$, we obtained the values of the Curie-Weiss temperatures (θ_{CW}) and effective magnetic moments for YMO-CS-B and YMO-CS-C samples listed in Table II. The presence of YMn_2O_5, secondary mixed valence manganese phase, reflects on the values of effective magnetic moment which lies in between values for spin-only Mn^{3+} (4.90 μ_B) and Mn^{4+} (3.87 μ_B). Even though both dominant phases present in the YMO-CS-B sample are antiferromagnetic at low temperature, the existence of secondary phase reflects on AFM long range order, leading to the loss of linearity of $M(H)$ curve.

Broader magnetic hysteresis loop is observed in samples sintered at higher temperature (YMO-CS-C) (Fig. 3a, Table II). The presence of strong bifurcation between ZFC and FC curves (Fig. 3b) and a cusp at 42 K in the ZFC part of the curve could indicate the existence of spin glass state in this sample, most likely due to the possible presence of the excess of manganese in that sample. Chen et. al. showed that even in cases with up to 10 wt% Mn excess, XRD analysis could detect only the presence of h-YMO [42], as is the case for the YMO-CS-C sample. If present in the sample, this amount of manganese ions in excess could

strongly influence the samples magnetic properties by favoring the ferromagnetic double-exchange over the AFM superexchange mechanism.

Although all aforementioned features could partially explain the presence of the hysteresis loops in the *M*(*H*) curves for the antiferromagnetic YMO, the loss of linearity in the *M*(*H*) curve could also arise from the presence of even very small amounts of Mn_3O_4 in the sintered YMO samples [43, 44]. In favor of this assumption are literature data concerning the magnetic properties of YMO single crystals in which weak ferromagnetism is absent [9]. On the other hand, previous studies reported similar values for the coercive field, the paramagnetic Curie–Weiss temperature and effective magnetic moment for the samples containing a small amount of Mn_3O_4 as in the case of YMO-CS-C [8]. To investigate the possible contamination of our samples with this phase, we compared our samples' remanent magnetizations with the remanent magnetization of pure commercial Mn_3O_4 [45], that exhibits a transition from paramagnetic to ferrimagnetic phase at 42 K, almost exactly at the measured cusp in ZFC curve of the YMO-CS-C. Knowing that the remanent magnetization of commercial Mn_3O_4 is 30 emu/g, we calculated the quantity of this oxide in YMO-CS-B and YMO-CS-C samples to be 0.013 % and 0.1 % respectively, which is far below the XRD detection limit. Nevertheless, we can conclude that YMO sintered by the conventional sintering process is basically antiferromagnetic, with violated antiferromagnetic order originating most likely from the presence of Mn_3O_4.

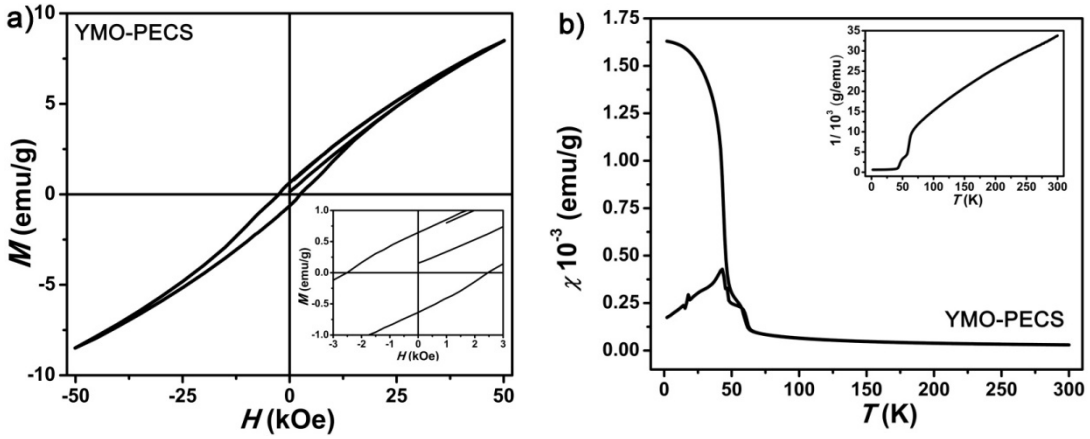

Fig. 4. Magnetic properties of the YMO-PECS ceramic sample: a) *M*(*H*) curve (insets show low field magnetization behaviour); b) Susceptibility as a function of temperature, ZFC and FC cycles, measured under an applied field of 100 Oe. (Inset shows the thermal evolution of the inverse susceptibility for YMO-PECS sample).

Magnetic properties of YMO-PECS ceramic samples are in complete agreement with the XRD results. Broader hysteresis in the *M*(*H*) curve and strong bifurcation between ZFC and FC curves along with calculated T_N ~ 43 K are results of the presence of strong ferrimagnetic Mn_3O_4 in the sample (Fig. 4, Table II). In order to confirm our findings on the effect of Mn_3O_4 in conventionally sintered YMO samples on their magnetic properties, we performed the same calculation process for the pulsed electric sintered sample. The results are in agreement with the results obtained by the Powder Cell program and indicate the presence of 2.2 wt. % Mn_3O_4 in the sample. In addition, to further investigate the cations content, we performed an ICP analysis on the YMO-PECS sample. The resulting molar ratio Mn : Y was 1.1, which is close to the 1.07, value obtained using XRD analysis data. This result indicates that excess of manganese present in the sample originates most likely from Mn_3O_4 impurity.

3.4 Ferroelectric properties

According to Khomskii, YMO belongs to the group of 'geometric' ferroelectrics, where ferroelectricity does not originate from the displacement of Mn ions but from the tilting of the MnO_5 bipyramids [28]. This tilting along the *c*-axis results in the formation of an electric dipole perpendicular to *the ab* plane, making ferroelectric polarization possible [46]. The scientific reports on the ferroelectric properties of polycrystalline YMO are very scarce, because of the issues with densification and cracking during sintering of this ceramic material.

Independently of the phase composition, the low density of the conventionally sintered samples and existence of cracks through the entire volume of the sintered samples volume, made the ferroelectric characterization of these samples impossible. Therefore, these measurements could be performed only on the YMO-PECS sample with high density and absence of cracks, and the results obtained in this study are comparable to literature reports [38,41]. Sharp $P(E)$ hysteresis loops (Fig. 5) along with low polarization at E=0 (P^0) and low field values (E^0) for P=0, indicate poor ferroelectric properties of this sample. For measurements with hysteresis period of 1 ms and for different applied fields, (P^0) and (E^0) values do not exceed 0,1 V/cm and 0,002 μC/cm^2, respectively. Even though PECSed YMO sample had significantly improved microstructure and density, the presence of secondary phase (i.e. 2.2% of Mn_3O_4) made strong influence on both magnetic and ferroelectric properties of YMO.

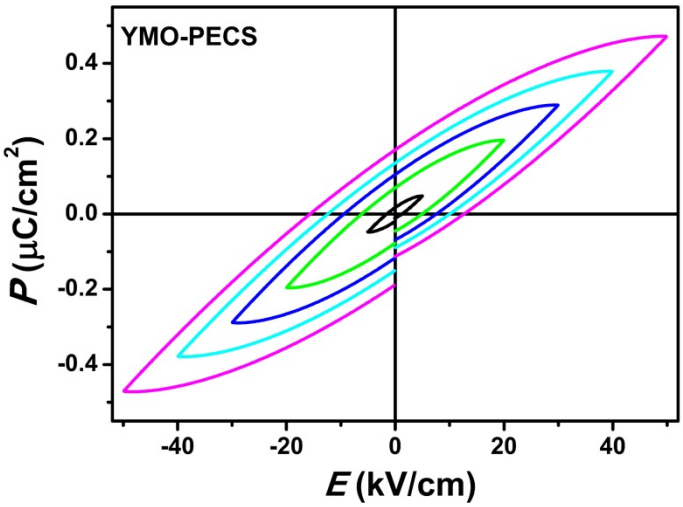

Fig. 5. Room temperature $P(E)$ curves of YMO-PECS sample under various applied electric fields.

4. Conclusion

Based on the results presented in this study we can conclude that dense, crack free $YMnO_3$ ceramic samples cannot be obtained by conventional sintering process, due to the various factors including phase transformations during heating and cooling and highly anisotropic thermal expansion coefficients. Pulsed electric current sintering with post-sintering annealing process of ceramic samples resulted in the $YMnO_3$ ceramic samples with significantly reduced cracks, reaching very high relative density of 99.8 %. All ceramic samples apart from the sintering process applied, show narrow magnetic hysteresis loop in $M(H)$ curve. Formation of Mn_3O_4, as a secondary phase is most likely the source of this weak ferromagnetic response below 43 K. The highest amount of Mn_3O_4 is present in the YMO-

PECS sample because of the reducing atmosphere in the PECS chamber in which the YMO-PP powder is sintered. As a result, the reduction of manganese from YMO occurs and Mn_3O_4 is formed. Cracks present in the conventionally sintered samples deteriorate samples ferroelectric properties, while pulsed electric current sintered samples reveal poor ferroelectric properties due to presence of the larger quantity of Mn_3O_4 secondary phases.

Acknowledgments

Milica Počuča-Nešić, Zorica Marinković Stanojević, Goran Branković and Zorica Branković acknowledge the financial support of the Ministry of Education, Science and Technological Development of the Republic of Serbia (Contract No. 451-03-9/2021-14/200053). Marko Jagodič acknowledges the financial support of the Slovenian Research Agency (Grant No. P2-0348). Miladin Radović, Rogelio Benitez, Goran Branković and Zorica Branković acknowledge financial support of the U.S. National Science Foundation for this work through Grant No. 1057155. The authors would like to acknowledge Dr. Biljana Dojčinović – Institute of Chemistry, Technology and Metallurgy, Centre of Chemistry, University of Belgrade, Serbia, for providing ICP analysis.

5. References

1. J. E. Medvedeva, V. I. Anisimov, M. A. Korotin, O. N. Mryasov, A. J. Freeman, J. Phys.: Condens. Matter, 12 (2000) 4947.
2. T. C. Han, W. L. Hsu, W. D. Lee, Nanoscale Res. Lett., 6 (2011) 201.
3. M. Tomczyk, A.M.O.R. Senos, I. M. Reaney, P. M. Vilarinho, Scripta Mater., 67 (2012) 427.
4. W. Prellier, M.P. Singh, P. Murugavel, J. Phys.: Condens. Matter, 17 (2005) R803-R832.
5. S. Filipović, N. Obradović, Lj. Andjelković, D. Olćan, J. Petrović, M. Mirković, V. Pavlović , D. Jeremić, B. Vlahović, A. Đorđević, Science of Sintering, 53 (2021) 1.
6. N. Stojanović, A. Kalezić-Glišović, A. Janićijević, and A. Maričić, Science of Sintering, 52, (2020) 163.
7. M. Chen, B. Hallstedt, L. J. Gauckler, J. Alloy. Compd., 393 (2005) 114.
8. B. B. Van Aken, J. W. G. Bos, R. A. de Groot, T.T. M. Palstra, Phys. Rev. B, 63 (2001) 125127.
9. N. A. Hill, J. Phys. Chem. B, 104 (2000) 6694.
10. H. W. Brinks, H. Fjellvåg, A. Kjekshus, J. Solid State Chem., 129 (1997) 334.
11. M. N Rao, N. Kaur, S. L. Chaplot, N. K. Gaur, R. K. Singh, J. Phys.: Condens. Matter, 21 (2009) 355402.
12. Z. J. Huang, Y. Cao, Y. Y. Sun, Y. Y. Xue, C. W. Chu, Phys. Rev. B, 56 (1997) 2623.
13. M. N. Iliev, H. G. Lee, V.N. Popov, M. V. Abrashev, A. Hamed, R. L. Meng, C. W. Chu, Phys. Rev. B, 56 (1997) 2488.
14. S. Ishiwata, Y. Tokunaga, Y. Taguchi, Y. Tokura, J. Am. Chem. Soc.,1 33 (2011) 13818.
15. W. R. Chen, F. C. Zhang, J. Miao, B. Xu, L. X. Cao, X. G. Qiu, B. R. Zhao, J. Phys.: Condens. Matter, 17 (2005) 8029.
16. B. Fu, W. Huebner, M. F. Trubelja, V. S. Stubican, J. Mater. Res., 9 (1994) 2645.
17. A. Alqat, Z. Gebrel, V. Kusigerski, V. Spasojevic, M. Mihalik, M. Mihalik, J. Blanusa, Ceram. Int., 39 (2013) 3183.

18. C. Zhang, J. Su, X. Wang, F. Huang, J. Zhang, Y. Liu, L. Zhang, K. Min, Z. Wang, X. Lu, F. Yan, J. Zhu, J. Alloy. Compd., 509 (2011) 7738.
19. R. D. Kumar, R. Jayavel, Mater. Lett., 113 (2013) 210.
20. H. W. Zheng, Y. F. Liu, W. Y. Zhang, S. J. Liu, H. R. Zhang, K. F. Wang, J. Appl. Phys., 107 (2010) 053901
21. G. Lescano, F. M. Figueiredo, F.M.B. Marques, J. Schmidt, J. Eur. Ceram. Soc., 21 (2001) 2037.
22. M. Počuča-Nešić, Z. Marinković Stanojević, Z. Branković, P. Cotič, S. Bernik, M. Sousa Góes, B.A. Marinković, J.A. Varela, G. Branković, Journal of Alloys and Compounds, 552 (2013) 451.
23. M. F. Zhang, J. M. Liu, Z. G. Liu, Appl. Phys. A, 79 (2004) 1753.
24. Teowee, G., McCarthy, K., McCarthy, F. et al., J. Sol-Gel Sci. Techn., 13 (1998) 899.
25. C. Moure, J. F. Fernandez, M. Villegas, P. Duran, J. Eur. Ceram. Soc., 19 (1999) 131.
26. Z. Zhang, S. Wang, J Mater Sci: Mater Electron., 28 (2017) 10940.
27. M. Tomczyk, A. M. Senos, P. M. Vilarinho, I. M. Reaney, Scripta Mater., 66 (2012) 288.
28. A. S. Gibbs, K. S. Knight, P. Lightfoot, Phys. Rev. B, 83 (2011) 094111.
29. Z. Branković, D. Luković Golić, A. Radojković, J. Ćirković, D. Pajić, Z. Marinković Stanojević, J. Xing, M. Radović, G. Li, G. Branković, Processing and Application of Ceramics, 10 [4] (2016) 257.
30. J. Vukašinović, M. Počuča-Nešić, D. Luković Golić, V. Ribić, Z. Branković, S. M. Savić, A. Dapčević, S. Bernik, M. Podlogar, M. Kocen, Ž. Rapljenović, T. Ivek, V. Lazović, B. Dojčinović, G. Branković, J Eur. Ceram. Soc., 40 (2020) 5566.
31. R. Davodi, M. Ardestani, A. Kazemi, Science of Sintering, 52 (2020) 245.
32. PowderCell W. Kraus, G. Nolze, PowderCell for Windows, V.2.4, Federal Institute for Materials Research and Testing, Berlin, Germany.
33. M. N. Iliev, M. V. Abrashev, H. G. Lee, V. N. Popov, Y. Y.Sun, C. Thomsen, R. L. Meng, C. W. Chu, Phys. Rev. B, 57 (1998) 2872.
34. V. E. Wood, A. E. Austin, E. W. Collings, K. C. Brog, J. Phys. Chem. Solids, 34 (1973) 859.
35. J. S. Zhou, J. B. Goodenough, J. M. Gallardo-Amores, E. Morán, M. A. Alario-Franco, R. Caudillo, Phys. Rev. B, 74 (2006) 014422.
36. A. Moure, T. Hungria, A. Castro, J. Galy, O. Pena, J. Tartaj, C. Moure, Mater. Chem. Phys., 133 (2012) 764.
37. T. Choi, Y. Horibe, H. T. Yi, Y. J. Choi, Weida Wu, S.-W. Cheong, Nature Mater., 9 (2010) 253.
38. S. H. Liu, J. C. A. Huang, X. Qi, W. J. Lin, Y. J. Siao et al., AIP Advances, 1 (2011) 03217.
39. L. B. Vedmid', A. M. Yankin, O. M. Fedorova, V. F. Balakirev, Russ. J. Inorg. Chem., 59 (2014) 519.
40. Y. Ma, Y. J. Wu, X. M. Chen, J. P. Cheng, Y. Q. Lin, Ceram. Int., 35 (2009) 3051.
41. M. Wang, T. Wang, S. Song, M. Ravi, R. Liu, S. Ji, Materials, 10 (2017) 474.
42. W. R. Chen, F. C. Zhang, J. Miao, B. Xu, X. L. Dong, L. X. Cao, X. G. Qiu, B. R. Zhao, P. Dai, Appl. Phys. Lett., 87 (2005) 042508.
43. A. Filippetti, N. A. Hill, J. Magn. Magn. Mater., 236 (2001) 176.
44. D. G. Tomuta, S. Ramakrishnan, G. J. Nieuwenhuys, J. A. Mydosh, J. Phys.: Condens. Matter, 13 (2001) 4543.
45. M. Počuča-Nešić, Z. Marinković Stanojević, Patricia Cotič Smole, A. Dapčević, N. Tasić, G. Branković, Z. Branković, Processing and Application of Ceramics, 13 [4] (2019) 427.

46. Y. Aikawa, T. Katsufuji, T. Arima, K. Kato, Phys. Rev. B,. 71 (2005) 184418.

Сажетак: *Интергрануларне и интрагрануларне пукотине које се обично јављају током синтеровања итријум-манганита ($YMnO_3$) отежавају процес повећања густине и нарушавају магнетна и фероелектрична својства керамичких узорака. У циљу превазилажења овог проблема, механохемијски синтетисани $YMnO_3$ прахови су синтеровани применом две различите методе: конвенционалним синтеровањем (CS) и синтеровањем пулсном електричном струјом (PECS). Сви узорци су карактерисани XRD, SEM и FESEM методама уз додатно испитивање њихових магнетних и фероелектричих својстава. Независно од њиховог фазог састава, у керамичким узорцима синтерованим конвенционалном методом долази до појаве пукотина кроз целокупну запремину материјала. Максимална релативна густина ових узорака износи 85%. Међутим, утврђено је да синтеровање PECS поступком значајно смањује присуство пукотина у керамичким узорцима чија релативна густина достиже 99.8 %.*
Кључне речи*: итријум-манганит, синтеровање пулсном електричном струјом, магнетна својства, микроструктура.*